

X-RAY FLARES: LATE INTERNAL AND LATE EXTERNAL SHOCKS

X. F. WU^{1,2,3,4}, Z. G. DAI³, X. Y. WANG³, Y. F. HUANG³, L. L. FENG^{1,2,4}, T. LU^{1,2,4}¹Purple Mountain Observatory, Chinese Academy of Sciences, Nanjing, 210008, China;

Email:xfwu@pmo.ac.cn, fengll@pmo.ac.cn, tlu@pmo.ac.cn

²National Astronomical Observatories, Chinese Academy of Sciences, Beijing, 100012, China;³Department of Astronomy, Nanjing University, Nanjing 210093, China;

Email:dzg@nju.edu.cn, xywang@nju.edu.cn, hyf@nju.edu.cn

⁴Joint Center for Particle Nuclear Physics and Cosmology (CPNPC), Nanjing 210093, China;*Draft version November 2, 2018*

ABSTRACT

We analyze several recently detected gamma-ray bursts (GRBs) with late X-ray flares in the context of late internal shock and late external shock models. We find that the X-ray flares in GRB 050421 and GRB 050502B originate from late internal shocks, while the main X-ray flares in GRB 050406 and GRB 050607 may arise from late external shocks. Under the assumption that the central engine has two periods of activities, we get four basic types of X-ray light curves. The classification of these types depends on which period of activities produces the prompt gamma-ray emission (Type 1 and Type 2: the earlier period; Type 3 and Type 4: the late period), and on whether the late ejecta catching up with the early ejecta happens earlier than the deceleration of the early ejecta (Type 1 and Type 3) or not (Type 2 and Type 4). We find that the X-ray flare caused by a late external shock is a special case of Type 1. Our analysis reveals that the X-ray light curves of GRBs 050406, 050421, and 050607 can be classified as Type 1, while the X-ray light curve of GRB 050502B is classified as Type 2. However, the X-ray light curve of GRB 050406 is also likely to be Type 2. We also predict a long-lag short-lived X-ray flare caused by the inner external shock, which forms when a low baryon-loading long-lag late ejecta decelerates in the non-relativistic tail of an outer external shock driven by an early ejecta.

Subject headings: gamma rays: bursts—X-rays: flares—shocks: relativistic

1. INTRODUCTION

In the pre-*Swift* era, only a few early optical afterglows of gamma-ray bursts (GRBs) were detected, while the observations of X-ray afterglows usually started at $\sim 10^4$ seconds after the prompt trigger. Since early afterglows contain important information about GRB central engines, understanding the early afterglows is therefore one of the most interesting scientific goals of the NASA's *Swift* satellite (Gehrels et al. 2004). After about one year of operations, a significant fraction of well localized GRBs have not been detected with early optical emissions down to moderate limiting magnitudes, although the UV/Optical Telescope (UVOT) on board *Swift* slewed to the error circle of position quickly after the burst (Roming et al. 2005). On the other hand, observations by the X-ray Telescope (XRT) on board *Swift* have revealed several new features of X-ray emissions. First, steep declines in some X-ray light curves at the transition from prompt phase to afterglow phase have been discovered, which are interpreted as tail emissions of prompt GRBs (Tagliaferri et al. 2005; Zhang et al. 2005; Nousek et al. 2005). Secondly, a portion of early X-ray afterglows have shallow-than-normal temporal decays before they enter “normal” decaying phase (Nousek et al. 2005; Zhang et al. 2005). Thirdly, late X-ray flares have been observed in several GRBs (Burrows et al. 2005a; see also Burrows et al. 2005b for a review). Piro et al. (2005) also reported that X-ray flares were discovered in a few GRBs (e.g., GRBs 011121 and 011211) by the Italian-Dutch *BeppoSAX* satellite. GRBs are usually divided into two main classes by their durations and spectral hardness ratios, i.e., long GRBs have durations

larger than 2 seconds and softer spectra while short GRBs have durations shorter than 2 seconds and harder spectra (Kouveliotou et al. 1993). Up to now, both long GRBs, including X-ray rich bursts and a high redshift burst (GRB 050904), and short GRBs have been found with late X-ray flares (Galli & Piro 2005; Watson et al. 2005; Fox et al. 2005; Barthelmy et al. 2005).

One leading explanation for the early shallow decaying X-ray afterglows is that the forward external shock has continuous energy injection from the long active central engine (Zhang et al. 2005; Nousek et al. 2005; Dai & Lu 1998a; Zhang & Mészáros 2002; Dai 2004; Wei, Yan & Fan 2005). Another leading explanation is that the Lorentz factor of the GRB ejecta has a distribution shaped by the central engine so that the behind slower material catches up with the ahead faster material when the latter is decelerated in the circum-burst medium, acting as a continuous energy injection (Zhang et al. 2005; Nousek et al. 2005; Rees & Mészáros 1998; Sari & Mészáros 2000; Zhang & Mészáros 2002; Granot & Kumar 2005). In this explanation the central engine does not need to be active for a long time (Granot & Kumar 2005). It is also possible that the early shallow decaying X-ray afterglows are caused by late continuous energy releases if the GRB ejecta is initially dominated by Poynting flux (Zhang & Kobayashi 2004).

As for X-ray flares, both late external shock model and late internal shock model have been proposed (Piro et al. 2005; Burrows et al. 2005; Fan & Wei 2005; Zhang et al. 2005). Piro et al. (2005) and Galli & Piro (2005) argued for the late external shock model because they found there is no obvious spectral evolution in some X-ray flares, while

Burrows et al. (2005b) preferred the late internal shock model based on several other X-ray flares which showed opposite features. These two conclusions are only based on their qualitative and empirical analysis. In this paper we quantitatively compare the X-ray flares with the predictions of the above two models. In Section 2 we describe the intrinsic X-ray light curves from the internal and external shocks. Then we analyze four GRBs with X-ray flares in Section 3 by comparing with the “delayed” (relative to the GRB trigger) intrinsic light curves of the late internal shock and late external shock. In Section 4 we establish four basic types of X-ray light curves, assuming that the central engine has two periods of activities. We also classify the four GRBs by these types. Our discussion and conclusions about X-ray flares are presented in Section 5.

2. INTRINSIC LIGHT CURVES OF INTERNAL AND EXTERNAL SHOCK EMISSIONS

Suppose that an intrinsic light curve of the internal/external shock emissions comprises an initial rise and a subsequent decay, which can approximately be described by the following broken power-law function of the observer’s time,

$$F_\nu = \begin{cases} F_{\nu,pk}(t/t_b)^{\alpha_1}, & t < t_b, \\ F_{\nu,pk}(t/t_b)^{\alpha_2}, & t > t_b, \end{cases} \quad (1)$$

where $\alpha_1 (> 0)$, $\alpha_2 (< 0)$ are the temporal indices before and after the peak time t_b , and $F_{\nu,pk}$ is the peak flux density correspondingly. The FWHM width of the rising and falling time scale of the light curve are $\delta t_r = (1 - 2^{-1/\alpha_1})t_b$ and $\delta t_f = (2^{-1/\alpha_2} - 1)t_b$, respectively.

In the internal shock model, two shells with a difference in Lorentz factor (Γ) $\Delta\Gamma \sim \Gamma \gg 1$ and a time delay Δt by the central engine collide at the radius $R_{\text{int}} \sim 2\Gamma^2 c \Delta t$ (Paczynski & Xu 1994). During the interaction of these two shells, the observed emission flux rises rapidly. The high time-resolution observations of single-pulse GRBs (e.g. GRB 971208, Connaughton et al. 1997) and main long pulses in usual GRBs reveal that the emission rises linearly with time, i.e., $\alpha_1 \sim 1$. One should keep in mind that this value is just empirical. The falling behavior of the light curve is mainly attributed to high-latitude emission (also known as tail emission) of the fireball, if the width of the fireball can be neglected (Fenimore, Madras & Nayakshin 1996; Kumar & Panaiteescu 2000). Let the co-moving flux density $F'_\nu \propto \nu'^\beta$ be uniform in the fireball, the observed flux density is $F_\nu \propto F'_\nu \mathcal{D}^2(d\Sigma/dt)$, where $\mathcal{D} = 1/\Gamma(1 - \cos\theta)$ is the Doppler factor and the surface area Σ satisfies $d\Sigma = 2\pi R_{\text{int}}^2 \sin\theta d\theta \propto d\theta^2$ (Panaiteescu et al. 2005). The time delay between photons emitted at an angle θ and those at the line of sight (LOS, $\theta = 0$) is $t - t_b = R_{\text{int}}(1 - \cos\theta)/c \approx R_{\text{int}}\theta^2/2c = (\theta\Gamma)^2\Delta t$, which further leads to $d\Sigma/dt = \text{constant}$ and $\mathcal{D} \approx 2\Gamma/[(t - t_b)/\Delta t + 1]$. Since $\nu' = \nu/\mathcal{D}$, the theoretical falling behavior of the internal shock emission is $F_\nu \propto \mathcal{D}^{2-\beta} \propto [(t - t_b)/\Delta t + 1]^{-(2-\beta)}$ (Kumar & Panaiteescu 2000), or exactly

$$F_\nu = F_{\nu,pk}[(t - t_b)/\Delta t + 1]^{-(2-\beta)}, \quad t_b < t. \quad (2)$$

The initial ($t_b < t < \Delta t + t_b$) decaying part of the light curve can be approximated by an exponential function of

time, i.e., $F_\nu \propto e^{-t/\tau}$, where $\tau = \Delta t/(2 - \beta) \sim \Delta t/3$. This behavior has been observed in most of GRBs. At late times ($t \gg \Delta t + t_b$), the tail emission decays as a power law function of time, $F_\nu \propto t^{-(2-\beta)}$, which has been confirmed by recent X-ray observations conducted during the prompt GRB phase by the *Swift* satellite (Tagliaferri et al. 2005; Nousek et al. 2005). The decaying time scale (FWHM) of internal shock emission is therefore $\delta t_f = [2^{1/(2-\beta)} - 1]\Delta t \sim (\ln 2)\tau$, not directly related to t_b . It should be noted that the observed $\delta t_r/\delta t_f$ is $\sim 0.3 - 0.5$ in prompt GRBs (Norris et al. 1996). The temporal index $\alpha_2 = d\ln F_\nu/d\ln t = (\beta - 2)t/(t - t_b + \Delta t)$, ranges from $-(2 - \beta)t_b/\Delta t$ at $t \sim t_b$ to $-(2 - \beta)$ when $t \gg t_b + \Delta t$. In general, the light curve of internal shock emission can be roughly depicted by eq. (1), especially for the rising and very late decaying portions with $\alpha_1 \sim 1$ and $\alpha_2 = -(2 - \beta)$.

In the external shock model, if the radial width of the GRB ejecta is smaller than a critical value (thin shell case), the peak time t_b is regarded as the deceleration time t_{dec} of the external shock sweeping into the circum-burst medium, driven by the ejecta. On the other hand, if the width of the ejecta is larger than that critical value (thick shell case), t_b is the observed crossing time of the reverse shock through the original GRB ejecta, which is about the width divided by the speed of light (Sari & Piran 1999). Since the typical Lorentz factor of electrons in the forward shock is much larger than that in the reverse shock, the X-ray emission in most common cases is dominated by the forward shock (Sari & Piran 1999; see, however, Fan & Wei 2005 and Kobayashi et al. 2005, for opposite cases under some extreme assumptions).

If the circum-burst environment is an interstellar medium (ISM), the reverse shock velocity is Newtonian or relativistic depending on whether the initial Lorentz factor Γ_i is smaller or larger than the critical value $\Gamma_c \approx 200E_{53}^{1/8} n_0^{-1/8} \Delta_{i,12}^{-3/8}$, where $n = n_0 \text{ cm}^{-3}$ is the ISM density, $E = 10^{53}E_{53}$ erg and $\Delta_i = 10^{12}\Delta_{i,12}$ cm are the isotropic-equivalent kinetic energy and initial width of the ejecta (Zhang, Kobayashi & Mészáros 2003). For the Newtonian reverse shock (NRS) case, the Lorentz factor of the forward shock roughly equals its initial value before the reverse shock crosses the ejecta, $\Gamma \approx \Gamma_i$. The minimum Lorentz factor of shock-accelerated electrons and co-moving magnetic field in the forward shock scale as $\gamma_m \propto \Gamma$ and $B \propto \Gamma n^{1/2}$ respectively, while the cooling Lorentz factor of electrons in the dynamical time scale is $\gamma_c \propto 1/t\Gamma^3 n$ (Sari, Piran & Narayan 1998). The characteristic frequencies and maximum flux density of the synchrotron radiation from the forward shock are $\nu_m \propto \Gamma \gamma_m^2 B \propto t^0$, $\nu_c \propto \Gamma \gamma_c^2 B \propto t^{-2}$, and $F_{\nu,\text{max}} \propto n R^3 \Gamma B \propto t^3$ (Sari & Piran 1999). For the relativistic reverse shock (RRS) case, the radius and Lorentz factor of the forward shock evolve as $R \propto t^{1/2}$ and $\Gamma \propto t^{-1/4}$, respectively (Kobayashi 2000). The characteristic frequencies and peak flux density in this case are $\nu_m \propto t^{-1}$, $\nu_c \propto t^{-1}$, and $F_{\nu,\text{max}} \propto t$. After the reverse shock crosses the ejecta, the forward shock emission is characterized by $\nu_m \propto t^{-3/2}$, $\nu_c \propto t^{-1/2}$ and $F_{\nu,\text{max}} \propto t^0$ (Sari, Piran & Narayan 1998). Table 1 summarizes the temporal indices α_1 and α_2 , and the corresponding spectral index β ($F_\nu \propto \nu^\beta$) of the forward shock emission in ISM. We can see that the flux density rises rapidly in the NRS case, while it rises quite slowly in the

RRS case. Note that in the RRS case if the crossing times t_m (when $\nu_m = \nu$) and t_c (when $\nu_c = \nu$) are both earlier than the time when the reverse shock crosses the ejecta, the peak time t_b should be the maximum of t_m and t_c . In such a special case, $\alpha_1 = 1/2$ ($t_c < t_m$) or $(3-p)/2$ ($t_c > t_m$), α_2 equals to $-(p-2)/2$ initially and then to $-(3p-2)/4$. The ratio of the rising to falling times $\delta t_r/\delta t_f$ in this case ranges from $\sim 10^{-3}$ to ~ 1 , and the spectral index changes from $-1/2$ or $-(p-1)/2$ to $-p/2$ around t_b .

If the circum-burst environment is a stellar wind with density $n = AR^{-2}$ ($A = 3 \times 10^{35} A_* \text{ cm}^{-1}$ is the wind parameter, Chevalier & Li 2000; Dai & Lu 1998b), the reverse shock velocity is Newtonian or relativistic depending on whether the initial Lorentz factor Γ_i is smaller or larger than the critical value $\Gamma_c \approx 65E_{53}^{1/4} A_*^{-1/4} \Delta_{i,12}^{-1/4}$ (Zou, Wu & Dai 2005). However, the Lorentz factor Γ of the forward shock remains to be a constant before the reverse shock crosses the ejecta, although $\Gamma \approx \Gamma_i$ for the NRS case while $\Gamma \ll \Gamma_i$ for the RRS case (Chevalier & Li 2000; Wu et al. 2003; Zou, Wu & Dai 2005). Since $R \propto t$, $n \propto t^{-2}$, $B \propto t^{-1}$, $\gamma_m \propto t^0$, and $\gamma_c \propto t$, we obtain $\nu_m \propto t^{-1}$, $\nu_c \propto t$ and $F_{\nu,\text{max}} \propto t^0$. After the reverse shock crosses the ejecta, the forward shock emission is characterized by $\nu_m \propto t^{-3/2}$, $\nu_c \propto t^{1/2}$ and $F_{\nu,\text{max}} \propto t^{-1/2}$ (Chevalier & Li 2000). Table 2 summarizes the temporal and spectral indices α_1 , α_2 , and β of the forward shock emission in a stellar wind. To reproduce an initial increasing flux density in the wind environment one must require $\nu_c < \nu < \nu_m$. If the time when ν_m equals to ν is earlier than the reverse shock crosses the ejecta, the peak time t_b should be t_m . In this case, $\alpha_1 = 1/2$, α_2 is equal to $-(p-2)/2$ initially and then to $-(3p-2)/4$, $\delta t_r/\delta t_f \sim 10^{-3} - 1$, and the spectral index changes from $-1/2$ to $-p/2$ at around t_b .

From the above analysis we can see that the simple internal or external shock models can not account for the observed X-ray flares with fast rising ($\alpha_1 \sim 10$) and rapid decay ($\alpha_2 \sim -10$) behavior.¹ We study the late internal shock (LIS) model and late external shock (LES) model for X-ray flares in detail and make a comparison between them case by case in particular flares in the next section.

3. TIME ZERO POINT EFFECT ON THE DELAYED INTERNAL/EXTERNAL SHOCK EMISSIONS

Assume there exists a time delay t_0 between the trigger of a GRB and the beginning of the above light curve as described by eq. (1). The influence of this time delay on the light curve is known as the time zero point effect (Huang, Dai & Lu 2002; Zhang et al. 2005). The physical reason and the conditions for the delay within the internal and external shock models will be presented in the next section. Here we make a quantitative analysis of this effect. Due to the time delay, the observed light curve plotted with the time zero point chosen as the GRB trigger is

$$F_{\nu} = \begin{cases} F_{\nu,pk}[(t - t_0)/t_b]^{\alpha_1}, & t_0 < t < t_{\text{peak}}, \\ F_{\nu,pk}[(t - t_0)/t_b]^{\alpha_2}, & t > t_{\text{peak}} \text{ (LES)}, \\ F_{\nu,pk}[(t - t_{\text{peak}})/\Delta t + 1]^{-(2-\beta)}, & t > t_{\text{peak}} \text{ (LIS)}, \end{cases} \quad (3)$$

¹We do not consider the effect of magnetization of GRB ejecta on the external shock emission, which may change the temporal indices moderately as compared to those listed in Tables 1 and 2 (Zhang & Kobayashi 2005). Nevertheless, this effect cannot explain the observed rapid rising and decaying features of X-ray flares.

where the peak time is changed to $t_{\text{peak}} = t_0 + t_b$. The observed temporal index of any segment of the light curve becomes (e.g., Huang, Dai & Lu 2002)

$$\alpha_{\text{obs}} \equiv \frac{d \ln F_{\nu}}{d \ln t} = \begin{cases} \frac{(\beta - 2)t}{t - t_{\text{peak}} + \Delta t}, & t > t_{\text{peak}} \text{ (LIS)}, \\ \frac{\alpha t}{t - t_0}, & \text{otherwise.} \end{cases} \quad (4)$$

Therefore, the observed temporal indices just before and after t_{peak} are $\alpha_{1,\text{obs}} = \alpha_1 t_{\text{peak}}/t_b$, $\alpha_{2,\text{obs}} = \alpha_2 t_{\text{peak}}/t_b$ (LES), and $\alpha_{2,\text{obs}} = (\beta - 2)t_{\text{peak}}/\Delta t$ (LIS) (see Fig. 1). When $t \gg t_{\text{peak}}$, the t_0 -shifted light curve approaches to the intrinsic one. The ratio $\delta t_f/t_{\text{peak}}$, which equals $(2^{-1/\alpha_2} - 1)t_b/t_{\text{peak}}$ in the LES model and $(2^{1/(2-\beta)} - 1)\Delta t/t_{\text{peak}}$ in the LIS model, is ~ 0.1 in all of the observed X-ray flares (Burrows et al. 2005a, b). This means that the time delay t_0 is much larger than t_b or Δt . A consequence of the time zero point effect is that there exists an anti-correlation between the two observed quantities α_{obs} and $\delta t/t_{\text{peak}}$,

$$\alpha_{1,\text{obs}} = B_1(\delta t_r/t_{\text{peak}})^{-1}, \quad \alpha_{2,\text{obs}} = B_2(\delta t_f/t_{\text{peak}})^{-1}, \quad (5)$$

where $B_1 = \alpha_1(1 - 2^{-1/\alpha_1})$ ranges from ~ 0.4 for $\alpha_1 = 1/2$ to ~ 0.6 for $\alpha_1 = 3$ and has an upper limit $B_1 \leq 0.69$, while $B_2 = \alpha_2(2^{-1/\alpha_2} - 1)$ varies from -1 for $\alpha_2 = -1$ (typical of LES) to -0.8 for $\alpha_2 = -3$ (typical of LIS, in which case α_2 in eq. [5] can be regarded as $\beta - 2$) and has an upper limit $B_2 \leq -0.69$. As can be seen in Fig. 1, the ratio of the peak flux density directly measured at t_{peak} to the one which is extrapolated from late time ($t \gg t_{\text{peak}}$) back to t_{peak} , or namely the flare increasing factor, is

$$A_m = \begin{cases} \left(\frac{\Delta t}{t_{\text{peak}}}\right)^{\beta-2} = \left(\frac{\beta-2}{\alpha_{2,\text{obs}}}\right)^{\beta-2}, & \text{LIS}, \\ \left(\frac{t_b}{t_{\text{peak}}}\right)^{\alpha_2} = \left(\frac{\alpha_2}{\alpha_{2,\text{obs}}}\right)^{\alpha_2}, & \text{LES}. \end{cases} \quad (6)$$

This value is also roughly equal to the ratio of $F_{\nu,pk}$ to $F_{\nu}(2t_{\text{peak}})$, as long as $t_0 \gg t_b$ or Δt . Note that for a given $\alpha_{2,\text{obs}}$, A_m has a maximum $A_{m,\text{max}} \approx 1.44^{-\alpha_{2,\text{obs}}}$ when $\alpha_2 \approx 0.37\alpha_{2,\text{obs}}$. In the late internal shock model, adopting $\beta - 2 \sim -3.0$ and $\delta t_f/t_{\text{peak}} \sim 0.1$, the flare increasing factor is typically $A_m \sim 20$. Because the late time emission is dominated by the external shock, the measured $A_{m,\text{obs}}$ can be either larger or smaller than this theoretical value, depending on whether the backward extrapolated flux density of the external shock emission at t_{peak} is smaller or larger than that of the LIS emission at this time. To reduce the deviation from the theoretical A_m influenced by the external shock emission, the observed $A_{m,\text{obs}}$ may be better determined by the ratio of $F_{\nu}(t_{\text{peak}})$ to $F_{\nu}(2t_{\text{peak}})$, rather than the value extrapolated from the late time light curve. In the late external shock model, however, the measured A_m reflects the true ratio. The value of α_2 can be directly determined by the post-flare light curve. Taken typical $\alpha_2 \sim -1$ and $\delta t_f/t_{\text{peak}} \sim 0.1$, we obtain $A_m \sim 10$ for typical LES X-ray flares.

Hence, once we know α_1 , α_2 , δt_r , δt_f , t_{peak} and $A_{m,\text{obs}}$ of a particular X-ray flare, the intrinsic values of α_1 , α_2 ,

t_b and t_0 are over-determined. Together with the spectral information during the flare, we can tightly constrain the X-ray flare models. As the X-ray spectral information is often contained in the ratio of the count rate in hard band to that in soft band (the so called hardness ratio H/S), we convert this ratio to the spectral index β with Fig. 2. Below we present our case studies for X-ray flares using available data in the literature.

GRB 050406— The observed quantities are $\alpha_{1,\text{obs}} = -\alpha_{2,\text{obs}} = 6.8$, $t_{\text{peak}} = 213$ s, $\delta t_r \approx \delta t_f = 0.20^{+0.14}_{-0.05} t_{\text{peak}}$, and $A_{m,\text{obs}} \sim 6$ (Romano et al. 2005; Burrows et al. 2005). Using eq (5) we obtain $\alpha_2 = -0.56^{+0.40}_{-0.23}$, consistent with $\alpha_2 \sim -0.88$ estimated by eq (6). However, it is impossible for the flare to have a highly symmetric light curve with $\delta t_r = \delta t_f$ and $\alpha_{1,\text{obs}} = -\alpha_{2,\text{obs}}$, unless $\alpha_1 = -\alpha_2$ approaches to infinity. If we do not take seriously on the property of the rising behavior and adopt $\alpha_2 \sim -0.88$, then we get $t_b = 28$ s and $t_0 = 185$ s. The hardness ratio of this X-ray afterglow evolves from 0.4 ± 0.3 initially to 1.3 ± 0.3 at the peak of the hard band (1–10 keV) light curve, and finally decreases to a level of ~ 0.7 after the peak time of the soft band (0.1–10 keV) light curve. This corresponds to the spectral index β being $-0.7^{+0.8}_{-0.3}$, $0.0^{+0.2}_{-0.1}$, and ~ -0.3 respectively. The late internal shock model is disfavored in this burst due to the fact that $\alpha_2 = \beta - 2$ is significantly smaller than ~ -0.88 , unless $\beta \sim 1.1$ which is impossible as indicated by the observations. Although the derived α_2 favors the late external shock model, the detected spectral evolution is difficult to be explained in this model (see Table 1).

GRB 050421— There are two early X-ray flares residing on a $F_\nu \propto t^{-3.1}$ light curve. The first stronger flare peaks at $t_{\text{peak}} = 111 \pm 2$ s since the trigger, while the second weaker flare peaks at $t = 154$ s (Godet et al. 2005). The other observed quantities of the first flare are $\delta t_r \approx \delta t_f = 0.07 t_{\text{peak}}$, and $A_{m,\text{obs}} \sim 4$ (Godet et al. 2005). Because the superposed $t^{-3.1}$ decaying light curve, which lasts at least 500 s since the burst trigger, must have a different origin to the two flares, the late external shock model for the flare can be ruled out in this burst. For the late internal shock model, the intrinsic $A_m \geq A_{m,\text{obs}}$ requires $0.27 \leq 2 - \beta \leq 8.8$, which can be easily satisfied. Assuming $\beta = -1.0$, the intrinsic A_m of the first flare is ~ 50 . Therefore the tail emission of this flare at late times is about 12 times dimmer than the superposed $t^{-3.1}$ emission, which may originate from the tail of the prompt GRB. The value of t_b of the first flare can not be well constrained.

GRB 050502B— There are two X-ray flares in this burst. Here we just discuss the first very large flare peaking at $t_{\text{peak}} = 740$ s since the trigger. Other observed quantities of this flare are $\alpha_{1,\text{obs}} = -\alpha_{2,\text{obs}} = 9.5$, and $A_{m,\text{obs}} \sim 500$. The rising and falling times satisfy $\delta t_r/t_{\text{peak}} \sim 0.2$, $\delta t_f/t_{\text{peak}} \sim 0.1$, and $\delta t/t_{\text{peak}} \ll 1$ for the spike at the peak of the hard band emission (Burrows et al. 2005a, b; Falcone et al. 2005). The hardness ratio decreases slowly from ~ 1.8 (corresponding to $\beta \sim 0.1$) when $t \sim 550$ s to ~ 0.7 ($\beta \sim -0.4$) for $t \geq 850$ s and has a minor peak at the peak of the hard band (1–10 keV) light curve of the large flare. The measured $A_{m,\text{obs}}$ is too large to be explained, since the theoretical maximum $A_{m,\text{max}} \approx 33$ (when $\alpha_2 = 3.5$) is much smaller than

this value. The only way to resolve such a problem is that the basic assumption on the flare light curve (i.e., eqs. [1] & [3]) is oversimplified, as has been directly indicated by observations (Chincarini et al. 2005). The late external shock model is ruled out directly in this GRB because this basic assumption is quite reasonable, and because the pre-flare light curve can be connected with the post-flare light curve smoothly by a single power law function of time ($F_\nu \propto t^{-0.8}$). The late internal shock explanation for this flare is possible, if the flux density during the whole decay phase is described by a pure exponential function of time, $F_\nu = F_{\nu,\text{pk}} \exp[-(t - t_{\text{peak}})/\tau]$. The flare increasing factor in this case is $A_m = F_{\nu,\text{pk}}/F_\nu(2t_{\text{peak}}) = \exp(t_{\text{peak}}/\tau)$. Combining with the observed value, we get the decay time scale $\tau \approx 0.16 t_{\text{peak}} = 120$ seconds. The equivalent temporal decaying index $\alpha_{2,\text{obs}} = t/\tau$ at $t = t_{\text{peak}}$ and at $t = 2t_{\text{peak}}$ is equal to -6.2 and to -12.4 , which is consistent with the observed overall decaying index -9.5 . The ratio $\delta t_f/t_{\text{peak}} = (\ln 2)\tau/t_{\text{peak}} \approx 0.11$ also matches the observation. Although the exponential decay assumption for the LIS model can explain this large flare, the physical reason of this assumption, or equivalently, why the $t^{-(2-\beta)}$ tail emission is not detected in this flare, has still not been answered.

GRB 050607— This burst has been detected with two early X-ray flares. The first flare is a weaker one. We focus on the second larger flare peaking at $t_{\text{peak}} = 310$ s since the trigger. Other observed quantities of this flare are $\alpha_{1,\text{obs}} \approx 16$, $\alpha_{2,\text{obs}} \approx -6.5$, $\delta t_r \ll \delta t_f \approx 0.2 t_{\text{peak}}$, and $A_{m,\text{obs}} \approx 20$ (Pagani et al. 2005). The hardness ratio (defined as $(H - S)/(H + S)$ for this burst, Pagani et al. 2005) decreases slowly from ~ 0.25 ($\beta \sim 0.3$) at the beginning of the second flare to ~ -0.25 ($\beta \sim -0.25$) at the end of this flare. Using $\alpha_{2,\text{obs}}$, $\delta t_f/t_{\text{peak}}$ and $\alpha_{1,\text{obs}}$, we find $\alpha_2 \sim -0.6$, $t_b \approx 0.09 t_{\text{peak}} = 29$ s, $t_0 = 281$ s, and $\alpha_1 \sim 1.5$. The inferred value of α_2 favors the late external shock explanation, since in the late internal shock model $\alpha_2 = \beta - 2$ is much smaller than -0.6 . The inferred α_2 is also consistent with the observed temporal index $\alpha_2 = -0.58 \pm 0.07$ of the post-flare light curve before $t \sim 1.2 \times 10^4$ s (Burrows et al. 2005b). However, the measured $A_{m,\text{obs}}$ is a little larger than the theoretical maximum $A_{m,\text{max}} \approx 11$ when $\alpha_2 = -2.4$, and even larger than the derived $A_m = 4.2$ using $\alpha_2 \sim -0.6$ by a factor of 5. This poses a severe crisis to the late external shock model explanation.

4. SEQUENCE OF LATE ACTIVITIES BY CENTRAL ENGINES

The X-ray flares, happened at $\sim 10^2$ s to 10^4 s since the trigger of prompt γ -ray emission in the burster's rest frame, are believed to originate from prolonged activities of the central engine. Such prolonged activity may be due to long-lived intermittent accretion of fragmented materials (or blobs) to the central black hole. Fragmentation may take place either in the stellar core of the progenitor during its collapse, or in the accretion disk surrounding the black hole due to gravitational instability at large radii of the disk (King et al. 2005; Perna, Armitage & Zhang 2005). Below we discuss possible sequences of central engine activities in the context of the LIS/LES models.

4.1. Collision between the Early and Late Ejecta

Let us first consider that the central engine has been active for two periods. This is the basic picture for us to understand both prompt GRBs and late X-ray flares. The time interval between the beginnings of these two periods is denoted as t_{lag} . During each activity, the central engine ejects one shell whose isotropic-equivalent kinetic energy, final mean bulk Lorentz factor and shell width are E_j , Γ_{j0} and Δ_{j0} , respectively. We adopt $j = e$ to denote the early ejected shell, while $j = l$ to denote the late ejected shell. Each shell may not be uniform and have a variable speed $\Delta\Gamma_{j0} \sim \Gamma_{j0}$ and variability time scale $\Delta t_j \ll \Delta_{j0}/c$, which are required to produce prompt gamma-ray emission by internal shocks within the shell.

In the following, instead of discussing internal shocks within the shells, we first study the types of the collision between the early and late ejecta, which depend on whether this collision happens before or after the deceleration of the early shell in the surrounding medium.² The deceleration radius of the early shell is

$$R_{\text{dec},e} = \begin{cases} 1.3 \times 10^{17} E_{e,53}^{1/3} \Gamma_{e,0,2}^{-2/3} n_0^{-1/3} \text{cm,} & \text{ISM,} \\ 4.0 \times 10^{15} E_{e,53} \Gamma_{e,0,2}^{-2} A_*^{-1} \text{cm,} & \text{wind.} \end{cases} \quad (7)$$

Subsequently, we define the deceleration time in the observer's frame by $t_{\text{dec},e} = R_{\text{dec},e}/2\Gamma_{e0}^2 c$. Generally, the deceleration time t_{dec} is proportional to $E^{1/(3-k)} \Gamma_0^{-2(4-k)/(3-k)}$, where $k = 0$ corresponds to the ISM environment while $k = 2$ corresponds to the wind environment ($n \propto R^{-k}$). We would like to point out that, only the prompt gamma-ray burst originates from internal shocks within the early ejecta and the collision between the early and late ejecta happens later than the deceleration of the early ejecta, and then the arrival time of photons emitted from the external shock at $R_{\text{dec},e}$ driven by the early ejecta since the GRB trigger is $t_{\text{dec},e}$. Usually, there are two types of the collision between the early and late ejecta. As we show later, if the time interval between these two ejecta is large enough (e.g., $t_{\text{lag}} \sim 10^5$ seconds), a new type of collision exists, i.e., the late ejecta is decelerated when it catches up and sweeps into the non-relativistic tail matter of the forward shock driven by the early ejecta. We call this type of collision the *inner external shock*. Below we give a quantitative analysis about these three types.

(i) *internal shock* — This happens when the late ejecta is faster and it collides with the early ejecta before the latter is decelerated, i.e., $\Gamma_{l0} > \Gamma_{e0}$ and $R_{\text{col}} < R_{\text{dec},e}$. Here

$$R_{\text{col}} \approx 2\Gamma_{e0}^2 c(t_{\text{lag}} - \Delta_{e0}/c) \quad (8)$$

is the radius when these two shells begin to collide with each other, and $ct_{\text{lag}} - \Delta_{e0}$ is the distance from the head of the late shell and the tail of the early shell. The second condition also reads $t_{\text{lag}} < t_{\text{dec},e} + \Delta_{e0}/c$, which requires the early ejecta having a very high energy E_e or a relatively low initial Lorentz factor Γ_{e0} . Because both ejecta are cold, this collision is the same as typical internal shocks which are responsible for prompt GRBs.

After the internal shock has finished, the two ejecta merge into one shell with energy $E_m \approx E_e + E_l$ and bulk Lorentz factor $\Gamma_{m0} = \sqrt{(E_e + E_l)/(E_e/\Gamma_{e0}^2 + E_l/\Gamma_{l0}^2)}$. For simplicity we here neglect the energy loss taken away

by radiation. The property of the subsequent afterglow is determined by the property of the merged shell. If $E_e > E_l$, the merged shell is dominated by the early ejecta with $E_m \sim E_e$ and $\Gamma_{m0} \sim \Gamma_{e0}$. The deceleration radius of the merged shell in the circum-burst environment is $R_{\text{dec},m} \sim R_{\text{dec},e}$, or equivalently, the deceleration time is $t_{\text{dec},m} = R_{\text{dec},m}/2\Gamma_{m0}^2 c \sim t_{\text{dec},e}$. If $E_e < E_l < (\Gamma_{l0}^2/\Gamma_{e0}^2)E_e$, the energy of the merged shell is $E_m \sim E_l$ while the Lorentz factor is $\Gamma_{m0} \sim \sqrt{E_l/E_e} \Gamma_{e0}$. In this case the deceleration radius and time are $R_{\text{dec},m} \sim R_{\text{dec},e}$ and $t_{\text{dec},m} \sim (E_e/E_l)t_{\text{dec},e}$, respectively. If $(\Gamma_{l0}^2/\Gamma_{e0}^2)E_e < E_l$, the merged shell is dominated by the late ejecta with $E_m \sim E_l$ and $\Gamma_{m0} \sim \Gamma_{l0}$. The deceleration radius and time of the merged shell are $R_{\text{dec},m} \sim R_{\text{dec},l} > R_{\text{dec},e}$ and $t_{\text{dec},m} \sim t_{\text{dec},l}$. From the above analysis, we can see that the afterglow may not have the same origin as the prompt γ ray emission, if the latter is assumed to originate from internal shocks within the early ejecta.

(ii) *refreshed shock* — This happens when the time lag between the early and late ejecta by the central engine is quite large, $t_{\text{lag}} > t_{\text{dec},e} + \Delta_{e0}/c$, or the late ejecta has a lower Lorentz factor relative to the early ejecta ($\Gamma_{l0} \leq \Gamma_{e0}$) while the time lag is not large ($t_{\text{lag}} \leq t_{\text{dec},e}$). Therefore, the collision between these two ejecta happens after the deceleration of the early ejecta. The hydrodynamic evolution of the external shock driven by the early ejecta after its deceleration follows the Blandford-McKee solution (Blandford & McKee 1976),

$$\Gamma_e^2 = \Gamma_{e0}^2 \left(\frac{R_e}{R_{\text{dec},e}} \right)^{-(3-k)}. \quad (9)$$

The external shock, or blast wave, can be approximated as a thin shell with a width $\Delta R_e = R_e/2(3-k)\Gamma_e^2$. When the late ejecta catches up with the tail of the thin shell at R_{col} , the external shock reaches $R_e = R_{\text{col}} + \Delta R_e$ with a Lorentz factor $\Gamma_e \approx \Gamma_e(R_{\text{col}})$. In the rest frame of the central engine, the time elapsed since the first ejection by the central engine is $t_{\text{elapse}} = R_{\text{dec},e}/\beta_{e0}c + \int_{R_{\text{dec},e}}^{R_e} dR/\beta_e c$, where $\beta = \sqrt{1 - 1/\Gamma^2}$ is the speed in units of c . This time can also be estimated by the late ejecta, i.e., $t_{\text{elapse}} = R_{\text{col}}/\beta_{l0}c + t_{\text{lag}}$. Equaling these two elapsed times, we obtain

$$\left[\frac{7-2k}{2(3-k)(4-k)\Gamma_e^2(R_{\text{col}})} - \frac{1}{2\Gamma_{l0}^2} \right] \frac{R_{\text{col}}}{c} = \left(t_{\text{lag}} - \frac{3-k}{4-k} t_{\text{dec},e} \right), \quad (10)$$

or

$$\frac{7-2k}{3-k} \frac{t_{\text{col}}}{t_{\text{dec},e}} - \frac{\Gamma_{e0}^2}{\Gamma_{l0}^2} \left(\frac{t_{\text{col}}}{t_{\text{dec},e}} \right)^{1/(4-k)} = \frac{t_{\text{lag}}}{t_{\text{dec},e}} - \frac{3-k}{4-k}, \quad (11)$$

where $t_{\text{col}} = R_{\text{col}}/2(4-k)\Gamma_e^2(R_{\text{col}})c$ is the observed time since the detection of first photons emitted by the early ejecta and thus is larger than $t_{\text{dec},e}$. For $\Gamma_{l0} > \Gamma_{e0}$, since the second term on the left side of the above equation can always be neglected, the collision happens at

$$t_{\text{col}} \simeq \frac{3-k}{7-2k} \left(t_{\text{lag}} - \frac{3-k}{4-k} t_{\text{dec},e} \right), \quad (12)$$

² For simplicity we just consider the thin shell case for the reverse shock propagating into the early shell. The thick shell case could be extended in the same way.

which is almost independent on the ratio Γ_{l0}/Γ_{e0} . This means that the time when the two ejecta begin to collide detected in the observer's frame directly measures the time lag t_{lag} of these two ejections by the central engine. On the other hand, for $\Gamma_{l0} \ll \Gamma_{e0}$, the collision happens at

$$t_{\text{col}} \simeq \begin{cases} \left(\frac{3-k}{7-2k} \frac{\Gamma_{e0}^2}{\Gamma_{l0}^2} \right)^{(4-k)/(3-k)} t_{\text{dec},e}, & t_{\text{lag}} < t_{\text{lag,crit}}, \\ \frac{3-k}{7-2k} \left(t_{\text{lag}} - \frac{3-k}{4-k} t_{\text{dec},e} \right), & t_{\text{lag}} > t_{\text{lag,crit}}, \end{cases} \quad (13)$$

where the critical value of t_{lag} for a given ratio Γ_{l0}/Γ_{e0} is $t_{\text{lag,crit}} \simeq [(3-k)/(7-2k)]^{1/(3-k)} (\Gamma_{e0}/\Gamma_{l0})^{2(4-k)/(3-k)} t_{\text{dec},e}$. Therefore, if the late ejecta moves slower than the early ejecta, we can use the collision time t_{col} to constrain the contrast between the Lorentz factors of these two ejecta when t_{lag} is small, or to directly obtain t_{lag} when it is large.

The strength of the collision is dependent on the ratio of Γ_{l0} to $\Gamma_e(R_{\text{col}})$. For the cases of $\Gamma_{l0} > \Gamma_{e0}$ and of $\Gamma_{l0} < \Gamma_{e0}$ while $t_{\text{lag}} > t_{\text{lag,crit}}$, we obtain $\Gamma_{l0}/\Gamma_e(R_{\text{col}}) = (\Gamma_{l0}/\Gamma_{e0})[(3-k)t_{\text{lag}}/(7-2k)t_{\text{dec},e}]^{(3-k)/2(4-k)}$, which is larger than $[(3-k)/(7-2k)]^{1/2}$. On the other hand, for the case of $\Gamma_{l0} < \Gamma_{e0}$ while $t_{\text{lag}} < t_{\text{lag,crit}}$, we get $\Gamma_{l0}/\Gamma_e(R_{\text{col}}) = [(3-k)/(7-2k)]^{1/2}$. Therefore, a violent collision requires the initial Lorentz factor of the late ejecta much larger than that of the early ejecta, or the time interval between these ejecta by the central engine long enough (see also Zhang & Mészáros 2002). A forward shock propagating into the downstream fluid of the external shock and a reverse shock propagating into the late ejecta are developed during this collision. Since the total energy of the external shock is increased after the two have merged as a whole, the collision is also known as the refreshed shock. To produce an obvious variability, flattening or bump in the afterglow light curve by the refreshed shock requires that the energy in the late ejecta must be comparable to or larger than that in the early ejecta, or equivalently, in the initial external shock (Kumar & Piran 2000; Zhang & Mészáros 2002). Because the very complicated shock jump conditions arises when considering the forward shock sweeping into a relativistical hot medium, the duration of the whole collision must be calculated numerically, and it is often found to be much longer than t_{col} in the observer's frame. Typical signatures from refreshed shocks therefore can not be directly used to explain X-ray flares (see figures in Zhang & Mészáros 2002). However, these signatures are naturally expected to appear in afterglow light curves after X-ray flares are over and remnants of X-ray flares as late ejecta will collide with the ahead external shock.

(iii) *inner external shock* — Above we take the approximation that the gas in the external shock driven by the early ejecta is compressed into a thin shell with a single bulk Lorentz factor. In fact, according to Blandford & McKee (1976), the distributions of the Lorentz factor γ_{BM} and the number density n_{BM} (in the observer's frame) of shocked media can be described as simple functions of the self-similar variable χ ,

$$\gamma_{\text{BM}} = 2^{-1/2} \Gamma_e \chi^{-1/2}, \quad n_{\text{BM}} = 2 \Gamma_e^2 \chi^{-(7-2k)/(4-k)} n, \quad (14)$$

where $\chi = 1 + 2(4-k)(\Delta R/R_e) \Gamma_e^2$, $\Delta R = R_e - r_e$ is the

radial distance of the shocked media to the shock front, and $n = AR^{-k}$ is the circum-burst media density. Far behind the shock front, say $r_e \leq R_e/2$, a uniform cavity or bubble is shaped with the number density,

$$n_{\text{bub}} = \begin{cases} 3.7 \times 10^{-5} E_{e,53}^{-3/4} n_0^{7/4} R_{e,17}^{9/4} \text{cm}^{-3}, & \text{ISM}, \\ 5.6 \times 10^2 E_{e,53}^{-1/2} A_*^{3/2} R_{e,15}^{-3/2} \text{cm}^{-3}, & \text{wind}. \end{cases} \quad (15)$$

Note that this bubble is cool and quasi-static. The shocked media with $\gamma_{\text{BM}} \simeq 1$ is located at $r_{e,n} = [(15-4k)/(16-4k)]R_e$. The total mass in the non-relativistic tail of the external shock is

$$M_{e,n} = \int_0^{r_{e,n}} 4\pi r^2 n_{\text{BM}} m_p dr = C_k \Gamma_e^{2(k-3)/(4-k)} M_{\text{sw}}, \quad (16)$$

where $M_{\text{sw}} = 4\pi n m_p R_e^3 / (3-k)$ is the mass of swept circum burst media, and the coefficient $C_k = 0.96$ for $k = 0$ and $C_k = 0.43$ for $k = 2$.

Suppose that the late ejecta reaches $r_{e,n}$ while still not being decelerated in the non-relativistic tail of the external shock. In the rest frame of the central engine, the time elapsed since the first ejection by the central engine is $t_{\text{elapse}} = R_{\text{dec},e}/\beta_{e0}c + \int_{R_{\text{dec},e}}^{R_e} dR/\beta_e c$. It is also equal to $t_{\text{elapse}} = r_{e,n}/\beta_{l0}c + t_{\text{lag}}$. Assuming Γ_{l0} , Γ_e much larger than unity, we have $r_{e,n} \simeq (15-4k)c[t_{\text{lag}} - (3-k)t_{\text{dec},e}/(4-k)]$, or the external shock radius $R_e \simeq 4(4-k)c[t_{\text{lag}} - (3-k)t_{\text{dec},e}/(4-k)]$. Since $R_e > R_{\text{dec},e}$, the time lag between the two ejections is required to be very long,

$$t_{\text{lag}} > \Gamma_{e0}^2 t_{\text{dec},e} / [2(4-k)]. \quad (17)$$

For example, adopting $\Gamma_{e0} \sim 100$ and $t_{\text{dec},e} \sim 100$ s, we require $t_{\text{lag}} \geq 1$ day. This long lag challenges the most popular central engine models for GRBs, however, it is supported by recent observations (e.g., Fox et al. 2005 for an X-ray flare happened at 16 days after the short burst GRB 050709). Now we turn to derive the critical value of Γ_{l0} , i.e., $\Gamma_{l0,\text{crit}}$. A late ejecta with this critical Γ_{l0} will be decelerated exactly at $R_{\text{dec},l} = r_{e,n}$, where $R_{\text{dec},l}$ is the deceleration radius of the late ejecta. Using $E_l/\Gamma_{l0,\text{crit}}^2 c^2 = M_{e,n}$ and $E_e \approx M_{\text{sw}} \Gamma_e^2 c^2$, we get

$$\begin{aligned} \Gamma_{l0,\text{crit}} &\approx \left(\frac{E_l}{E_e} \right)^{1/2} \Gamma_e^{(7-2k)/(4-k)} \\ &\approx \left(\frac{E_l}{E_e} \right)^{1/2} \Gamma_{e0}^{7-2k} \left[\frac{t_{\text{dec},e}}{2(4-k)t_{\text{lag}}} \right]^{(3-k)(7-2k)/[2(4-k)]} \end{aligned} \quad (18)$$

where C_k is ignored for simplicity. Late ejecta with same t_{lag} but $\Gamma_{l0} > \Gamma_{l0,\text{crit}}$ will be decelerated before reaching $r_{e,n}$, i.e., $R_{\text{dec},l} < r_{e,n}$. Therefore, the external shock driven by the late ejecta and propagating into the non-relativistic tail of the outer external shock are called the *inner external shock*. Since the mass in the bubble within $R_{\text{dec},l}$ is equal to $M_{e,n}(R_{\text{dec},l}/r_{e,n})^3$, the deceleration radius of the late ejecta is $R_{\text{dec},l} = r_{e,n}(E_l/M_{e,n} \Gamma_{l0}^2 c^2)^{1/3}$. Again, letting the elapsed time $R_{\text{dec},e}/\beta_{e0}c + \int_{R_{\text{dec},e}}^{R_e} dR/\beta_e c$ equal to $R_{\text{dec},l}/\beta_{l0}c + t_{\text{lag}}$, we obtain the radius of the outer external shock when the late ejecta has been just deceler-

ated,

$$R_e \simeq \begin{cases} 4(4-k)ct_{\text{lag}} \left(\frac{\Gamma_{l0,\text{crit}}}{\Gamma_{l0}} \right)^{2(4-k)/[(3-k)(7-2k)]}, & \text{if } \Gamma_{l0,\text{crit}} < \Gamma_{l0} < D_k \Gamma_{l0,\text{crit}}, \\ ct_{\text{lag}}, & \text{if } D_k \Gamma_{l0,\text{crit}} < \Gamma_{l0}, \end{cases} \quad (19)$$

where $D_k = (15 - 4k)^{3/2} (16 - 4k)^{(2k^2 - 10k + 9)/(8-2k)}$ is $\sim 1.3 \times 10^3$ for $k = 0$ and ~ 3.9 for $k = 2$. The distance between the outer external shock and the late ejecta when the latter reaches its deceleration radius is always $R_e - R_{\text{dec},l} \simeq ct_{\text{lag}}$. Similar to the outer external shock, the X-ray emission from the inner external shock peaks at the moment of its deceleration. The time scale of the peak in the observer's frame is $\sim t_{\text{dec},l} = R_{\text{dec},l}/2\Gamma_{l0}^2 c$, which is much shorter than the lag time t_{lag} between the inner and outer shocks. Therefore, the observed emission from the inner external shock behaves as a very short spike. The inner external shock will finally catch up with the main part of the outer external shock. Because the gas just behind each external shock are both hot, strong forward and reverse shocks are hardly to be developed when they begin to collide.

In Fig. 3 we visualize the above three types of collision between the early and late ejecta. Assuming the properties of the early ejecta are known, the type of collision depends mainly on the ratio of the initial Lorentz factor of the late ejecta to that of the early ejecta, Γ_{l0}/Γ_{e0} , and on the time lag t_{lag} between these two ejections by the central engine. More details can be found in the caption of Fig. 3. Here we note that for the refreshed shock, the relative speed of the late ejecta in the rest frame of the outer external shock must be supersonic, i.e., larger than $c/\sqrt{3}$. This condition is equivalent to that the relative Lorentz factor, which is equal to $[\Gamma_{l0}/\Gamma_e(R_{\text{col}}) + \Gamma_e(R_{\text{col}})/\Gamma_{l0}]/2$ as long as Γ_{l0} and $\Gamma_e(R_{\text{col}})$ much larger than unity, must be greater than 1.22 (Zhang & Mészáros 2002). Therefore the criterion for forming a refreshed shock is $\Gamma_{l0}/\Gamma_e(R_{\text{col}}) > 1.92$. We can see from Fig. 3 that if the refreshed shock is strong, the observed beginning time of the collision directly scales to the time lag by $t_{\text{col}} \simeq [(3-k)/(7-2k)]t_{\text{lag}}$. This is especially important because only strong refreshed shocks can be easily detected by a brightening or flaring signature in the light curve. In the following we just consider the strong collision cases, including the internal shock case ($\Gamma_{l0} > \Gamma_{e0}$ and $t_{\text{lag}} < t_{\text{dec},e}$), and the strong refreshed shock cases ($\Gamma_{l0} > \Gamma_{e0}$ and $t_{\text{lag}} > t_{\text{dec},e}$, or $\Gamma_{l0} < \Gamma_{e0}$ and $t_{\text{lag}} > t_{\text{lag,crit}}$).

4.2. Types of X-ray light curves

Now let us turn to discuss the entire X-ray light curve from the early and late ejecta. Temporal variabilities in at least one of the two ejecta are required to produce the prompt GRBs. There are four basic types of X-ray light curves, depending on the prompt GRB emission originating from the early ejecta or from the late ejecta, as well as the collision between the two ejecta taking place earlier than the deceleration of the early ejecta or not.

Type 1 — Prompt gamma-ray burst arises from internal shocks in the early ejecta, and the collision between the early and late ejecta happens earlier than the deceleration of the early ejecta, i.e., $R_{\text{col}} < R_{\text{dec},e}$. This case

corresponds to $\Gamma_{l0} > \Gamma_{e0}$, and $t_{\text{lag}} < t_{\text{dec},e}$.

The prompt GRB is produced at the internal shock radius of the early ejecta, $R_{\text{int},e} \approx 2\Gamma_{e0}^2 c \Delta t_e$. If there is also time variability in the late ejecta, then a second burst will be produced by the internal shock within the late ejecta at $R_{\text{int},l} \approx 2\Gamma_{l0}^2 c \Delta t_l$. At this moment we have the equation for the elapsed times in the burster's frame, $R_{\text{int},e}/\beta_{e0} c + (R_{\text{GRB}} - R_{\text{int},e})/c = t_{\text{lag}} + R_{\text{int},l}/\beta_{l0} c$, where R_{GRB} is the radius of prompt gamma-ray photons when the internal shock of the late ejecta happens. The time interval between the beginnings of the two bursts, or the t_0 of the second burst, is

$$t_0(l) = \frac{R_{\text{GRB}} - R_{\text{int},l}}{c} = t_{\text{lag}} + \Delta t_l - \Delta t_e \approx t_{\text{lag}}. \quad (20)$$

When $R_{\text{int},l} > R_{\text{int},e}$, the main emission of the second burst is in the X-ray band and the internal shock of the late ejecta produces the first X-ray flare, providing $\Delta t_l \ll t_{\text{lag}}$. Since the light curves of most of observed X-ray flares are less structured, the late ejecta is required to be composed of a few (two or three) mini-shells. A second X-ray flare is unavoidable because of the collision between the early and late ejecta. The equation for the elapsed times at this collision is $R_{\text{int},e}/\beta_{e0} c + (R_{\text{GRB}} - R_{\text{int},e})/c = t_{\text{lag}} + R_{\text{col}}/\beta_{l0} c$, and R_{GRB} here is the radius of prompt gamma-ray photons when the two ejecta collide with each other. The t_0 of the second X-ray flare relative to the trigger of the prompt GRB is

$$t_0(c) = \frac{R_{\text{GRB}} - R_{\text{col}}}{c} \approx \left(1 + \frac{\Gamma_{e0}^2}{\Gamma_{l0}^2} \right) t_{\text{lag}} - \frac{\Gamma_{e0}^2}{\Gamma_{l0}^2} T_{\text{GRB}}, \quad (21)$$

where $T_{\text{GRB}} \approx \Delta_{e0}/c$ is the duration of GRB. After the collision, the merged shell with energy E_m and Lorentz factor Γ_{m0} sweeps into the circum-burst medium and will be decelerated at $R_{\text{dec},m}$. The maximal flux of X-ray emission of the afterglow is also produced at this radius. By using the equation for the elapsed times at the deceleration, $R_{\text{int},e}/\beta_{e0} c + (R_{\text{GRB}} - R_{\text{int},e})/c = t_{\text{lag}} + R_{\text{col}}/\beta_{l0} c + (R_{\text{dec},m} - R_{\text{col}})/\beta_{m0} c$, we have the peak time of the X-ray afterglow in the observer's frame,

$$\begin{aligned} t_{\text{pk}}(\text{AG}) &= \frac{R_{\text{GRB}} - R_{\text{dec},m}}{c} \\ &\approx \left(1 - \frac{\Gamma_{e0}^2}{\Gamma_{m0}^2} + \frac{\Gamma_{e0}^2}{\Gamma_{l0}^2} \right) t_{\text{lag}} + t_{\text{dec},m}, \end{aligned} \quad (22)$$

where we have assumed $\Delta_{e0}/c \ll t_{\text{lag}}$. As discussed in the last subsection, the property of the merged shell is determined by the energy ratio E_l/E_e . If $E_l < E_e$, since $\Gamma_{m0} \sim \Gamma_{e0}$ and $t_{\text{dec},m} \sim t_{\text{dec},e} > t_{\text{lag}}$, we have $t_{\text{pk}}(\text{AG}) \approx t_{\text{dec},m}$, which means that the t_0 effect can be neglected in this case. The prompt GRB and afterglow have the same origin. If $E_e < E_l < (\Gamma_{l0}^2/\Gamma_{e0}^2)E_e$, since $\Gamma_{m0} \sim \sqrt{E_l/E_e} \Gamma_{e0}$ and $t_{\text{dec},m} \sim (E_e/E_l)t_{\text{dec},e}$, we have $t_{\text{pk}}(\text{AG}) \approx (1 - E_e/E_l)t_{\text{lag}} + t_{\text{dec},m}$. The X-ray afterglow would behave as an X-ray flare only if $t_{\text{dec},m} \ll (1 - E_e/E_l)t_{\text{lag}}$, which requires $E_l/E_e \gg t_{\text{dec},e}/t_{\text{lag}}$ and $\Gamma_{l0}/\Gamma_{e0} \gg \sqrt{t_{\text{dec},e}/t_{\text{lag}}}$. Inversely, the X-ray afterglow does not suffer from the t_0 effect. If $(\Gamma_{l0}^2/\Gamma_{e0}^2)E_e < E_l$, since $\Gamma_{m0} \sim \Gamma_{l0}$ and $t_{\text{dec},m} \sim t_{\text{dec},l}$, we have $t_{\text{pk}}(\text{AG}) \approx t_{\text{lag}} + t_{\text{dec},m}$. The criterion for the X-ray afterglow to be an X-ray flare is

$t_{\text{dec},m} \ll t_{\text{lag}}$, or $E_l/E_e \ll (t_{\text{lag}}/t_{\text{dec},e})^{3-k}(\Gamma_{l0}/\Gamma_{e0})^{8-2k}$ and $\Gamma_{l0}/\Gamma_{e0} \gg \sqrt{t_{\text{dec},e}/t_{\text{lag}}}$. In conclusion, the late external shock model for X-ray flares requires the energy of the late ejecta is much larger than the energy of the early ejecta, and the ratio of initial Lorentz factors satisfies $\Gamma_{l0}/\Gamma_{e0} \gg \sqrt{t_{\text{dec},e}/t_{\text{lag}}}$. This model also implicitly requires a very low initial value of Γ_{e0} , because of $t_{\text{dec},e} > t_{\text{lag}} \sim 10^3 - 10^4$ seconds.

Type 2 — Prompt gamma-ray burst arises from internal shocks in the early ejecta, and the collision between the early and late ejecta happens later than the deceleration of the early ejecta, i.e., $R_{\text{col}} > R_{\text{dec},e}$. We just consider a strong refreshed shock being developed during the collision. This corresponds to the case of $\Gamma_{l0} > \Gamma_{e0}$, $t_{\text{lag}} > t_{\text{dec},e}$, or the case of $\Gamma_{l0} < \Gamma_{e0}$, $t_{\text{lag}} > t_{\text{lag,crit}} > t_{\text{dec},e}$.

Similar to the analysis in *Type 1*, the prompt gamma-ray emission is produced by internal shocks in the early ejecta at $R_{\text{int},e} \approx 2\Gamma_{e0}^2 c \Delta t_e$. In the observer's frame, the X-ray afterglow from the external shock driven by the early ejecta will peak at

$$t_{\text{pk}}(\text{AG}) = t_{\text{dec},e}. \quad (23)$$

If a second burst is produced by the internal shock within the late ejecta, then the t_0 for this burst is

$$t_0(l) \approx t_{\text{lag}}, \quad (24)$$

which means the second burst happens later than the deceleration of the early ejecta in the observer's frame. Subsequently, when the late ejecta begins to collide with the external shock originating from the early ejecta, the equation for the elapsed times is $(R_{\text{GRB}} - R_{\text{int},e})/c = (R_{\text{dec},e} - R_{\text{int},e})/\beta_{e0}c + \int_{R_{\text{dec},e}}^{R_e} dR/\beta_e c$, where $R_e = R_{\text{col}}[1 + 1/2(3-k)\Gamma_e^2(R_{\text{col}})]$. The t_0 of the refreshed shock emission relative to the prompt gamma-ray emission is

$$t_0(c) \approx \frac{7-2k}{3-k} t_{\text{col}} + \frac{3-k}{4-k} t_{\text{dec},e} = t_{\text{lag}}. \quad (25)$$

This means that the refreshed shock emission overlaps the internal shock emission from the late ejecta in the observer's frame.

Type 3 — Prompt gamma-ray burst arises from internal shocks in the late ejecta, and the collision between the early and late ejecta happens earlier than the deceleration of the early ejecta, i.e., $R_{\text{col}} < R_{\text{dec},e}$. This corresponds to the case of $\Gamma_{l0} > \Gamma_{e0}$, $t_{\text{lag}} < t_{\text{dec},e}$. Note that in this case the internal shock in the early ejecta is forbidden, otherwise this emission would precede the emission from internal shocks in the late ejecta by t_{lag} in the observer's frame and would trigger the detector. In other words, there should be no time variability in the early ejecta.

After producing the prompt GRB at $R_{\text{int},l} \approx 2\Gamma_{l0}^2 c \Delta t_l$, the late ejecta will collide with the early ejecta at the radius R_{col} . The equation for the elapsed times at the collision is $R_{\text{int},l}/\beta_{l0}c + (R_{\text{GRB}} - R_{\text{int},l})/c = R_{\text{col}}/\beta_{l0}c$. Therefore, the beginning time t_0 of this collision is

$$t_0(c) \approx \frac{\Gamma_{e0}^2}{\Gamma_{l0}^2} (t_{\text{lag}} - \Delta_{e0}/c), \quad (26)$$

which is smaller than the lag t_{lag} . When the collision is over, the early and late ejecta merge into a shell with energy E_m and Lorentz factor Γ_{m0} . The emission of X-ray

afterglow peaks when the merged shell reaches to its deceleration radius $R_{\text{dec},m}$. The equation for the elapsed time at the deceleration is $R_{\text{int},l}/\beta_{l0}c + (R_{\text{GRB}} - R_{\text{int},l})/c = R_{\text{col}}/\beta_{l0}c + (R_{\text{dec},m} - R_{\text{col}})/\beta_{m0}c$. The peak time of the X-ray afterglow in the observer's frame is

$$t_{\text{pk}}(\text{AG}) \approx t_{\text{dec},m} - \left(\frac{\Gamma_{e0}^2}{\Gamma_{m0}^2} - \frac{\Gamma_{e0}^2}{\Gamma_{l0}^2} \right) (t_{\text{lag}} - \Delta_{e0}/c). \quad (27)$$

Below we neglect the Δ_{e0}/c term for simplicity. If $E_l < E_e$, since $\Gamma_{m0} \sim \Gamma_{e0}$ and $t_{\text{dec},m} \sim t_{\text{dec},e} > t_{\text{lag}}$, we have $t_{\text{pk}}(\text{AG}) \approx t_{\text{dec},m} - t_{\text{lag}} \sim t_{\text{dec},m}$. If $E_e < E_l < (\Gamma_{l0}^2/\Gamma_{e0}^2)E_e$, since $\Gamma_{m0} \sim \sqrt{E_l/E_e}\Gamma_{e0}$ and $t_{\text{dec},m} \sim (E_e/E_l)t_{\text{dec},e}$, we have $t_{\text{pk}}(\text{AG}) \approx (E_e/E_l)(t_{\text{dec},e} - t_{\text{lag}}) \sim t_{\text{dec},m}$. If $(\Gamma_{l0}^2/\Gamma_{e0}^2)E_e < E_l$, since $\Gamma_{m0} \sim \Gamma_{l0}$ and $t_{\text{dec},m} \sim t_{\text{dec},l}$, we have $t_{\text{pk}}(\text{AG}) \approx t_{\text{dec},m}$. In conclusion, the t_0 effect for the light curve of X-ray afterglow can be neglected in this case.

Type 4 — Prompt gamma-ray burst arises from internal shocks in the late ejecta, and the collision between the early and late ejecta happens later than the deceleration of the early ejecta, i.e., $R_{\text{col}} > R_{\text{dec},e}$. We just consider a strong refreshed shock being developed during the collision. This corresponds to the case of $\Gamma_{l0} > \Gamma_{e0}$, $t_{\text{lag}} > t_{\text{dec},e}$, or the case of $\Gamma_{l0} < \Gamma_{e0}$, $t_{\text{lag}} > t_{\text{lag,crit}} > t_{\text{dec},e}$. As in *Type 3*, the internal shock in the early ejecta is forbidden.

The equation for the elapsed time when the early ejecta reaches its deceleration radius is $R_{\text{dec},e}/\beta_{e0}c = t_{\text{lag}} + R_{\text{int},l}/\beta_{l0}c + (R_{\text{GRB}} - R_{\text{int},l})/c$. The X-ray afterglow of the external shock driven by the early ejecta peaks at

$$t_{\text{pk}}(\text{AG}) = t_{\text{dec},e} - t_{\text{lag}} - \Delta t_l \approx t_{\text{dec},e} - t_{\text{lag}}. \quad (28)$$

This means that the peak emission of X-ray afterglow happens before the main gamma-ray burst in the observer's frame. Contrary to the above three types, the beginning time of this kind of X-ray afterglow relative to the prompt burst is negative, $t_0 = -t_{\text{lag}}$. The detected light curve of the X-ray afterglow behaves as

$$F_\nu = F_{\nu,pk} \left(\frac{t + t_{\text{lag}}}{t_{\text{dec},e}} \right)^{\alpha_2}, \quad (29)$$

where t is the time in the observer's frame since the trigger of the prompt burst, and $\alpha_2 \sim -1$ is the intrinsic temporal decaying index. The observed temporal index is $\alpha_{2,\text{obs}} = [t/(t + t_{\text{lag}})]\alpha_2$, which approaches zero when $t \ll t_{\text{lag}}$ while approaches α_2 when $t > t_{\text{lag}}$. Such a negative t_0 could explain the slowly decaying early X-ray afterglows recently discovered by the *Swift* satellite (Zhang et al. 2005; Nousek et al. 2005). Subsequently, when the late ejecta begins to collide with the external shock originating from the early ejecta, the equation for the elapsed times is $t_{\text{lag}} + R_{\text{int},l}/\beta_{l0}c + (R_{\text{GRB}} - R_{\text{int},l})/c = R_{\text{dec},e}/\beta_{e0}c + \int_{R_{\text{dec},e}}^{R_e} dR/\beta_e c$, where $R_e = R_{\text{col}}[1 + 1/2(3-k)\Gamma_e^2(R_{\text{col}})]$. The t_0 of the refreshed shock emission relative to the prompt gamma-ray emission is

$$t_0(c) \approx \frac{7-2k}{3-k} t_{\text{col}} - t_{\text{lag}} + \frac{3-k}{4-k} t_{\text{dec},e} \approx 0. \quad (30)$$

This means that the refreshed shock emission happens at nearly the same time with the prompt GRB produced by the internal shocks within the late ejecta in the observer's frame.

Fig. 4 shows the above four types of X-ray light curves. Some caveats must be given here. First, for *Types 1 & 2*, the internal shock within the late ejecta (thin solid lines) may not take place if there is no temporal variability in the late ejecta. Secondly, refreshed shocks are assumed to be strong in the figure (*Types 2 & 4*). Weak or mildly strong refreshed shocks will hardly influence the X-ray light curve. Thirdly, the temporal behavior of afterglow emission in *Types 1* light curve depends on the property of the merger of the two ejecta. It may behave as an X-ray flare if the property of the merger is determined by the late ejecta with $E_l > E_e$ and $\Gamma_{l0}/\Gamma_{e0} \gg (t_{dec,e}/t_{lag})^{1/2}$. This corresponds to the late external shock model. Otherwise the afterglow light curve is normal and its beginning happens when the prompt GRB is produced.

Now we begin to classify the observed X-ray light curves by using the above results. As discussed in Section 3, GRB 050406 has one X-ray flare with $t_{peak} = 213$ s. The derived intrinsic α_2 is ~ -0.56 . We note that the post-flare light curve behaves as $F_\nu \propto t^{-1.58 \pm 0.17}$ for $t < 10^3$ s and $F_\nu \propto t^{-0.50 \pm 0.14}$ for $t > \sim 4 \times 10^3$ s (Burrows et al. 2005; Romano et al. 2005). In principle, there are two possible explanations for this burst. In the first explanation, the X-ray light curve of GRB 050406 belongs to the *Type 1* light curve. The X-ray flare is caused by the late external shock. The intrinsic α_2 is consistent with the temporal index of the very late afterglow light curve. In the second explanation, the X-ray light curve belongs to the *Type 2* light curve. The X-ray flare is interpreted as the internal shock emission within the late ejecta. The deceleration time of the early ejecta satisfies $t_{dec,e} < 100$ s and the afterglow decays as $F_\nu \propto t^{-1.58}$. The collision between the late ejecta and the external shock must be weak or mildly strong because there is no obvious signature in the light curve just after the X-ray flare. In this explanation, we also need a continuous energy injection from $t \sim 4 \times 10^3$ s to explain the flattening of the light curve.

GRB 050421 definitely belongs to the *Type 1* light curve, because the two X-ray flares reside on a $F_\nu \propto t^{-3.1}$ emission background, which is the tail emission of the prompt gamma-ray burst. The first X-ray flare is naturally interpreted as from the internal shock within the late ejecta, while the second X-ray flare is from the subsequent internal shock between the late ejecta and the early ejecta. It is intriguing of this GRB that the tail emission lasts for about 10^3 s and the afterglow emission has not been detected.

The X-ray light curve of GRB 050502B is classified to be the *Type 2* light curve. The afterglow decays as $F_\nu \propto t^{-0.8}$ with the deceleration time $t_{dec,e} < 50$ s. The first X-ray flare peaks at $t_{peak} \approx 740$ s. The fluence of this X-ray flare is comparable with that of the prompt GRB. This means the energies contained in the late ejecta and in the early ejecta are comparable. One may expect a strong refreshed shock signature nearly simultaneously following this X-ray flare would be detected. However, a second X-ray flare has been detected, but it happened at $t \sim 4 \times 10^4$ s, much later than the first X-ray flare. This implies the refreshed shock is weak, which requires

the initial Lorentz factor of the late ejecta is smaller than that of the early ejecta, $\Gamma_{l0} < \Gamma_{e0}$, and the time lag is no longer than the critical value, $t_{lag} < t_{lag,crit}$, or $\Gamma_{l0}/\Gamma_{e0} < (t_{dec,e}/t_{lag})^{(3-k)/(8-2k)}$. Taken $t_{dec,e} \sim 30$ s and $t_{lag} \sim 300$ s, we have $\Gamma_{l0}/\Gamma_{e0} < 0.42$ for $k = 0$ (ISM) and $\Gamma_{l0}/\Gamma_{e0} < 0.56$ for $k = 2$ (wind). The second X-ray flare happens at $t \sim 0.5$ day requires another late ejecta by the central engine to catch up with the external shock and produce a strong refreshed shock.

GRB 050607 may belong to the *Type 1* light curve. The first weaker X-ray flare can be either from the internal shock within the late ejecta, or from the internal shock between the early and late ejecta. The second large X-ray flare is interpreted as the late external shock emission. However, as discussed in Section 3, the main disadvantage of this late external shock explanation is the theoretical flare increasing factor $A_m \sim 4$ is much smaller than the observed $A_{m,obs} \sim 20$.

5. DISCUSSION AND CONCLUSIONS

In this paper we have quantitatively analyzed late X-ray flares in the frameworks of the late internal shock model and late external shock model. As we have shown above, both the late internal shock model and late external shock model require late time activities of central engines. Some of previous works suggested the late internal shock origin for X-ray flares (Burrows et al. 2005a; Zhang et al. 2005; Fan & Wei 2005), while others suggested the late external shock origin (Piro et al. 2005; Galli & Piro 2005). In fact, these two kinds of late shocks can coexist within a certain gamma-ray burst. GRB 050607 may be such a possible candidate.

Here one caveat should be made for the late external shock model. An X-ray flare originating from the late external shock comes to being only if the prompt gamma-ray burst is produced by internal shocks within the early time ejecta, and the late time ejecta carries more energy than the early one and its initial Lorentz factor Γ_{l0} must be larger than the initial Lorentz factor of the early ejecta Γ_{e0} by a factor of $(t_{dec,e}/t_{lag})^{1/2} > 1$, where t_{lag} is the time separation between the two ejecta by the central engine and $t_{dec,e}$ is the deceleration time of the early ejecta in the circum-burst medium. The merger of the two ejecta is mainly dominated by the late ejecta with a much shorter deceleration time relative to $t_{dec,e}$. Therefore the beginning of the afterglow from the merger happens much later than the prompt GRB and the peak of afterglow behaves as an X-ray flare. Note this description of the late internal shock model is different from that in Piro et al. (2005) and Galli & Piro (2005). They attributed the late external shock to arise from a thick shell which is ejected by the long active central engine. Despite different descriptions, this model requires the t_0 effect in the afterglow emission. Given $t_0 \sim t_{lag}$, the smaller the deceleration time of the merger $t_{dec,m}$, the more remarkable the afterglow as an X-ray flare. Since $t_{dec,m} \propto E_m^{1/(3-k)} \Gamma_{m0}^{-2(4-k)/(3-k)}$, a large energy or especially a large Lorentz factor will easily cause an X-ray flare. This result has also been obtained by Galli & Piro (2005).

Theoretically, there are four basic types of X-ray light curves if the central engine has two periods of activities before it entirely ceases. According to our analysis, the

observed X-ray light curves of GRBs with X-ray flares all belong to *Type 1* or *Type 2*. This means the prompt gamma-ray emissions of these GRBs result from the early ejecta, while the late X-ray flares are produced by the internal shock within the late ejecta, by the internal shock between the early and late ejecta, or by the late external shock. The difference between *Type 1* and *Type 2* is that for the former the collision between the early and late ejecta happens before the deceleration of the early ejecta, while for the latter the situation is inverse. One may wonder where are *Type 3* and *Type 4* X-ray light curves? In these two types, the prompt gamma-ray burst is produced from the late ejecta. There would be no internal shocks within the early ejecta, or these internal shock emission is too weak to be detected. It is also possible that the internal shock emission within the early ejecta is very weak and regarded as the precursor of the main burst. According to our classification, *Type 3* X-ray light curves correspond to the case that the collision between the early and late ejecta takes place before the deceleration of the early ejecta. The emission from the collision has a small time lag relative to the prompt gamma-ray emission and can be regarded as the last pulse of the prompt GRB. The afterglow emission in *Type 3* hardly suffers the t_0 effect. Therefore it is hard to distinguish *Type 3* X-ray light curves from the light curves in which the central engine has only one active period. However, *Type 4* X-ray light curves may have already been detected. Some of recently discovered X-ray afterglows whose initial decay is extraordinarily slow may originate from this type.

In this paper we also investigate a new kind of collision between the early and late ejecta, the *inner external shock*. Such a shock will be developed when the late ejecta is decelerated by the non-relativistic tail of the outer external shock, which is driven by the early ejecta. To develop the inner external shock requires the time lag t_{lag} between these two ejecta is very long, typically ≥ 1 day, and the baryon loading of the late ejecta is very low, or equivalently, its initial Lorentz factor must be larger than a critical value. Since the required t_{lag} is not very extreme compared to recent discoveries and the low baryon loading is also plausible, the inner external shock maybe exist. Because the time scale of emission from this shock in the observer's frame is equal to its deceleration time and therefore is much shorter than t_{lag} , the emission behaves as a short spike. Detecting such a spike in the typical afterglow time scale ($t \sim t_{\text{lag}} \sim 1$ day) is quite difficult. We therefore just make a prediction of the inner external shock emission in this paper, and have not considered such kind of emission in the above four basic X-ray light curves.

For simplicity we have only considered the central engine having two periods of activities. In reality the central engine may have more than two periods of activities. The multiple X-ray flares detected in the high redshift gamma ray burst GRB 050904 indicate that the central engine of this burst has been active for many periods (Watson et al. 2005; Cusumano et al. 2005). Cusumano et al. (2005) reported that the hardness ratio for $t > 100$ s is nearly a constant, $H(14-73\text{keV})/S(1.4-14\text{keV}) \sim 0.2$, which corresponds to $\beta \sim -0.9$. The X-ray light curves from multiple ejections by the central engine are complicated and difficult to be classified. As for GRB 050904, Zou, Xu & Dai (2005) found that ordered late internal shocks formed by collisions between late ejecta and the earliest ejecta can reproduce the temporal evolution of peak luminosity of X-ray flares and the entire X-ray spectral evolution.

At last we would like to point out other ways besides those developed in this paper (see Section 3) to distinguish an X-ray flare caused by a late external shock from other X-ray flares in the same GRB by late internal shock(s). As we know in most pulses of GRBs it is found that higher energy photons arrive to the observer earlier than lower energy photons (e.g., Chen et al. 2005). This is the spectral-lag phenomenon. Fenimore et al. (1995) found that the width W of peaks in prompt GRBs tends to be narrower at higher photon energy E , i.e., $W \propto E^{-0.4}$. This is called the spectral-width relationship. If these two phenomena have been detected in a particular X-ray flare, then the X-ray flare can be proved to originate from a late internal shock. Statistics help us to understand X-ray flares. In prompt GRBs, several relationships have been found, such as the isotropic gamma-ray released energy E_{iso} and spectral peak photon energy E_p relationship (Amati et al. 2002), the peak luminosity L_p and spectral peak photon energy E_p relationship (Yonetoku et al. 2004), the peak luminosity L_p and spectral time lag τ relationship (Norris, Marani & Bonnell 2000). Moreover, Liang, Dai & Wu (2004) found there exists a relationship between the flux and E_p within a GRB with time resolved spectra (see also Borgonovo & Ryde 2001). Therefore, investigating the above relations in X-ray flares is urgent since it can provide direct evidence that whether late X-ray flares and prompt GRBs have the same mechanism.

This work was supported by the National Natural Science Foundation of China (grants 10573036, 10503012, 10473023, 10403002, 10233010, and 10221001), the Special Funds for Major State Basic Research Projects, and the Foundation for the Authors of National Excellent Doctoral Dissertations of China (project 200125).

REFERENCES

Amati, L., et al. 2002, A&A, 390, 81
 Barthelmy, S. D., et al. 2005, Nature, 438, 994
 Blandford, R. D., & McKee, C. F. 1976, Phys. Fluids, 19, 1130
 Borgonovo, L., & Ryde, F. 2001, ApJ, 548, 770
 Burrows, D. N., et al. 2005a, Science, 309, 1833
 Burrows, D. N., et al. 2005b, astro-ph/0511039
 Chen, L., Lou, Y. Q., Wu, M., Qu, J. L., Jia, S. M., & Yang, X. J. 2005, ApJ, 619, 983
 Chevalier, R. A., & Li, Z. Y. 2000, ApJ, 536, 195
 Chincarini, G., et al. 2005, astro-ph/051107
 Connaughton, V., Kippen, R. M., Preece, R., & Hurley, K. 1997, IAUC, 6785, 1
 Cusumano, G., et al. 2005, Nature submitted, astro-ph/0509737
 Dai, Z. G., & Lu, T. 1998a, PRL, 81, 4301
 Dai, Z. G., & Lu, T. 1998b, MNRAS, 298, 87
 Dai, Z. G. 2004, ApJ, 606, 1000
 Falcone, A., et al. 2005, ApJ submitted
 Fan, Y. Z., & Wei, D. M. 2005, MNRAS, 364, L42
 Fenimore, E. E., in't Zand, J. J. M., Norris, J. P., Bonnel, J. T., & Nemiroff, R. J. 1995, ApJ, 448, L101
 Fenimore, E. E., Madras, C. D., & Nayakshin, S. 1996, ApJ, 473, 998
 Fox, D. B., et al. 2005, Nature, 437, 845
 Galli, A., & Piro, L. 2005, A&A, submitted, astro-ph/0510852
 Gehrels, N., et al. 2004, ApJ, 611, 1005
 Godet, O., et al. 2005, A&A submitted

Granot, J., & Kumar, P. 2005, MNRAS Letters accepted, astro-ph/0511049

Huang, Y. F., Dai, Z. G., & Lu, T. 2002, MNRAS, 332, 735

King, A., O'Brien, P. T., Goad, M. R., Osborne, J., Olsson, E., & Page, K. 2005, ApJ, 630, L113

Kobayashi, S. 2000, ApJ, 545, 807

Kobayashi, S., Zhang, B., Mészáros, P., & Burrows, D. 2005, ApJ Letters submitted, astro-ph/0506157

Kouveliotou, C., et al. 1993, ApJ, 413, L101

Kumar, P., & Panaiteescu, A. 2000, ApJ, 541, L51

Kumar, P., & Piran, T. 2000, ApJ, 532, 286

Liang, E. W., Dai, Z. G., & Wu, X. F. 2004, ApJ, 606, L29

Norris, J. P., et al. 1996, ApJ, 459, 393

Norris, J. P., Marani, G. F., & Bonnell, J. T. 2000, ApJ, 534, 248

ousek, J. A., et al. 2005, ApJ submitted, astro-ph/0508332

Paczynski, B., & Xu, G. H. 1994, ApJ, 427, 708

Pagani, C., et al. 2005, ApJ submitted

Panaiteescu, A., Mészáros, P., Gehrels, N., Burrows, D., & Nousek, J. 2005, MNRAS submitted, astro-ph/0508340

Perna, R., Armitage, P. J., & Zhang, B. 2005, ApJL accepted, astro-ph/0511506

Piro, L., et al. 2005, ApJ, 623, 314

Rees, M. J., & Mészáros, P. 1998, ApJ, 496, L1

Romano, P., et al. 2005, A&A submitted

Roming, et al., 2005, Nature submitted, astro-ph/0509273

Sari, R., Piran, T., & Narayan, R. 1998, ApJ, 497, L17

Sari, R., & Piran, T. 1999, ApJ, 520, 641

Sari, R., & Mészáros, P. 2000, ApJ, 535, L33

Tagliaferri, G., et al. 2005, Nature, 436, 985

Watson, D., et al. 2005, ApJL in press, astro-ph/0509640

Wei, D. M., Yan, T., & Fan, Y. Z. 2005, ApJL accepted, astro-ph/0511154

Wu, X. F., Dai, Z. G., Huang, Y. F., & Lu, T. 2003, MNRAS, 343, 1131

Yonetoku, D., Murakami, T., Nakamura, T., Yamazaki, R., Inoue, A. K., & Ioka, K. 2004, ApJ, 609, 935

Zhang, B., & Mészáros, P. 2002, ApJ, 566, 712

Zhang, B., Kobayashi, S., & Mészáros, P. 2003, ApJ, 595, 950

Zhang, B., & Kobayashi, S. 2005, ApJ, 628, 315

Zhang, B., et al. 2005, ApJ accepted, astro-ph/0508321

Zou, Y. C., Wu, X. F., & Dai, Z. G. 2005, MNRAS, 363, 93

Zou, Y. C., Xu, D., & Dai, Z. G. 2005, ApJL submitted, astro-ph/0511205

TABLE 1
TEMPORAL AND SPECTRAL INDICES ($F_\nu \propto t^\alpha \nu^\beta$) OF THE FORWARD SHOCK EMISSION IN ISM

regime	β	$t < t_b$ (NRS)	$t < t_b$ (RRS)	$(t > t_b)$	$\delta t_r / \delta t_f$ (NRS vs RRS)
		α_1	α_1	α_2	
$\nu < \nu_c < \nu_m$	1/3	11/3	4/3	1/6	none
$\nu < \nu_m < \nu_c$	1/3	3	4/3	1/2	none
$\nu_c < \nu < \nu_m$	-1/2	2	1/2	-1/4	0.02 vs 0.05
$\nu_m < \nu < \nu_c$	$-(p-1)/2$	3	$(3-p)/2$	$-3(p-1)/4$	0.18 vs 0.71
$\max\{\nu_m, \nu_c\} < \nu$	$-p/2$	2	$-(p-2)/2$	$-(3p-2)/4$	0.35 vs none

NOTE.—The indices are derived under the assumptions that the hydrodynamics is adiabatic and the emission is from the synchrotron radiation of shock-accelerated electrons, whose initial energy distribution follows $dN/d\gamma_e \propto \gamma_e^{-p}$. The ratio $\delta t_r / \delta t_f$ is estimated by assuming the observing band in the same spectral regime around t_b and adopting $p = 2.2$.

TABLE 2
TEMPORAL AND SPECTRAL INDICES ($F_\nu \propto t^\alpha \nu^\beta$) OF THE FORWARD SHOCK EMISSION IN STELLAR WIND

regime	β	α_1 ($t < t_b$)	α_2 ($t > t_b$)	$\delta t_r / \delta t_f$
$\nu_c < \nu < \nu_m$	$-1/2$	$1/2$	$-1/4$	0.05
$\nu_m < \nu < \nu_c$	$-(p-1)/2$	$-(p-1)/2$	$-(3p-1)/4$	none
$\max\{\nu_m, \nu_c\} < \nu$	$-p/2$	$-(p-2)/2$	$-(3p-2)/4$	none

NOTE.—Similar to Table 1 except for a stellar wind environment. The theoretical α_1 in the case of $\nu_m < \nu < \nu_c$ is also presented in the table, although ν_c is usually below ν_m and the X-ray frequency for typical parameter values.

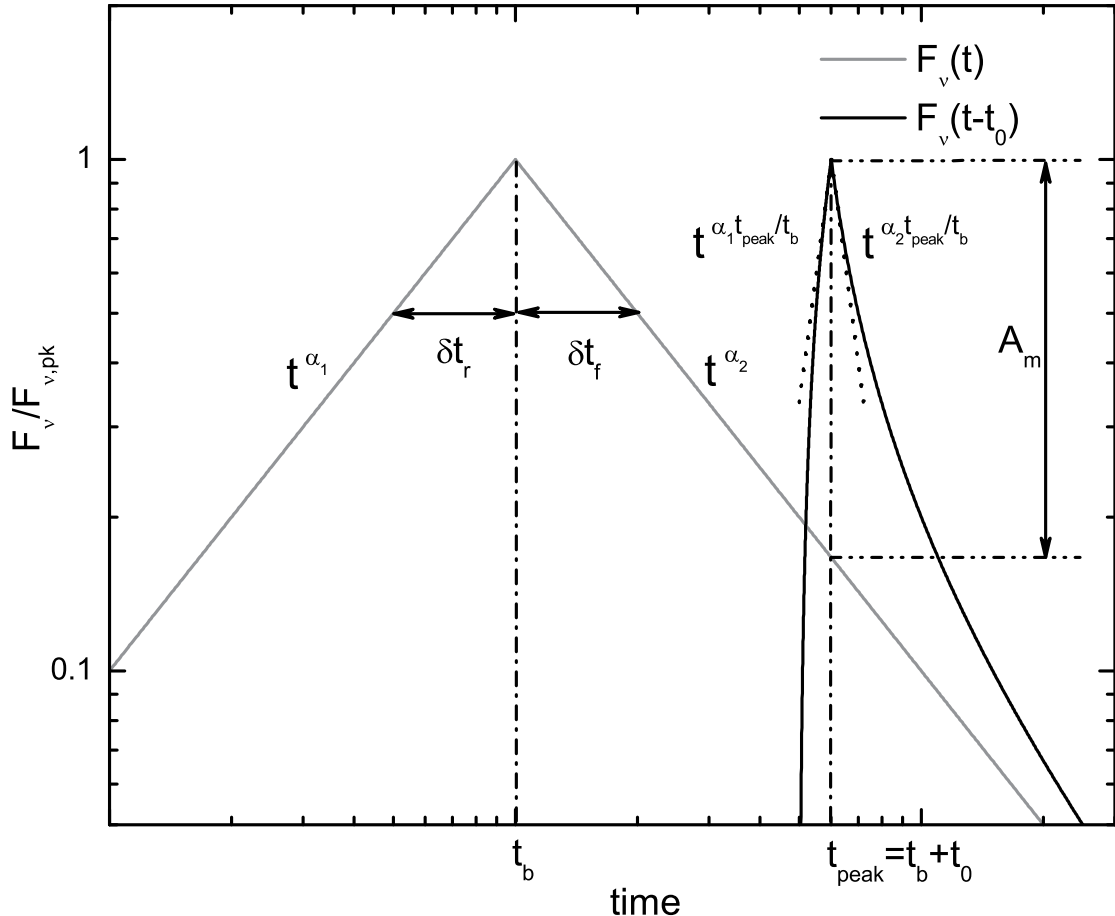


FIG. 1.— The light curve in grey describes the intrinsic temporal evolution of the emissions from one internal or external shock. The light curve in black peaked at t_{peak} is the time-shifted intrinsic light curve by t_0 . The parameters are defined in the text.

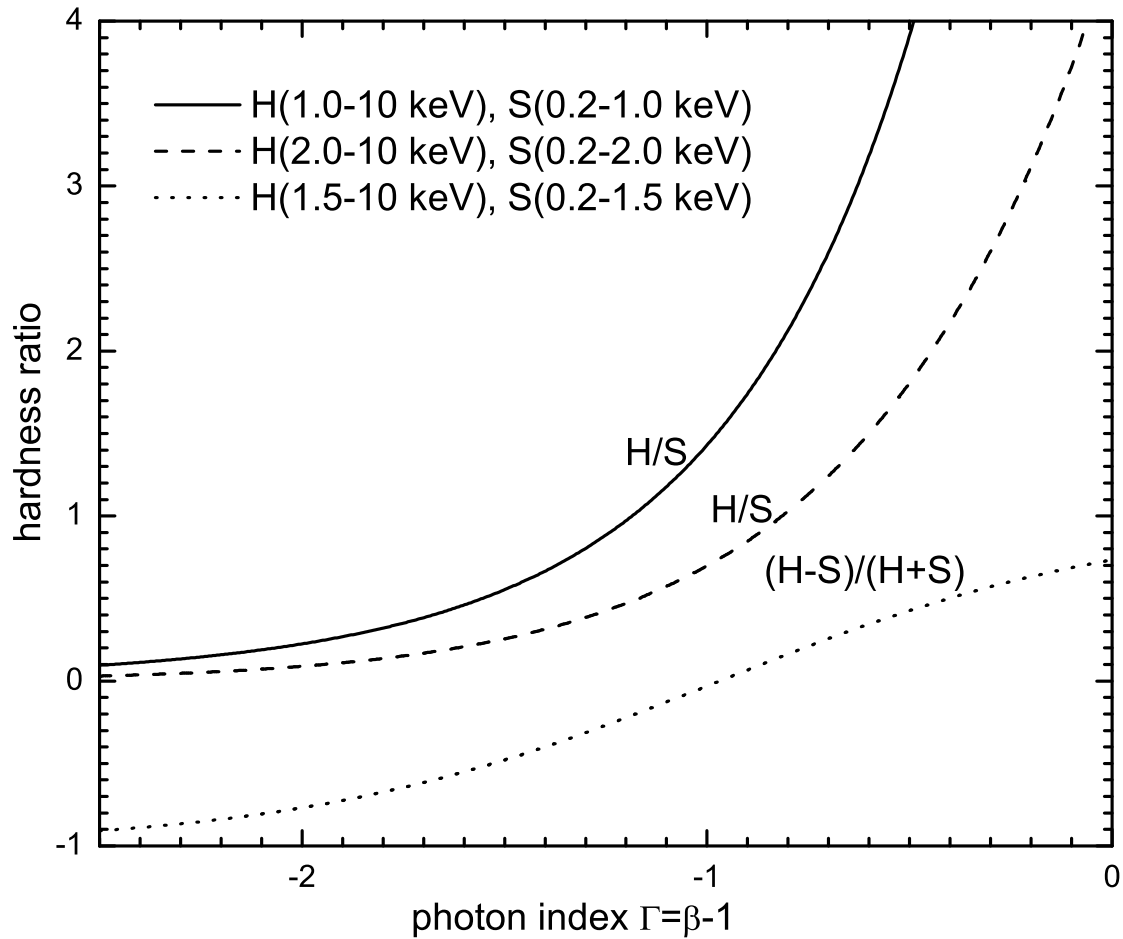


FIG. 2.— Hardness ratio (ratio of the hard-band count rate to soft-band count rate) as a function of the effective photon index Γ , assuming the $0.2 - 10$ keV spectrum can be fitted by one single power-law $F_\nu \propto \nu^\beta$.

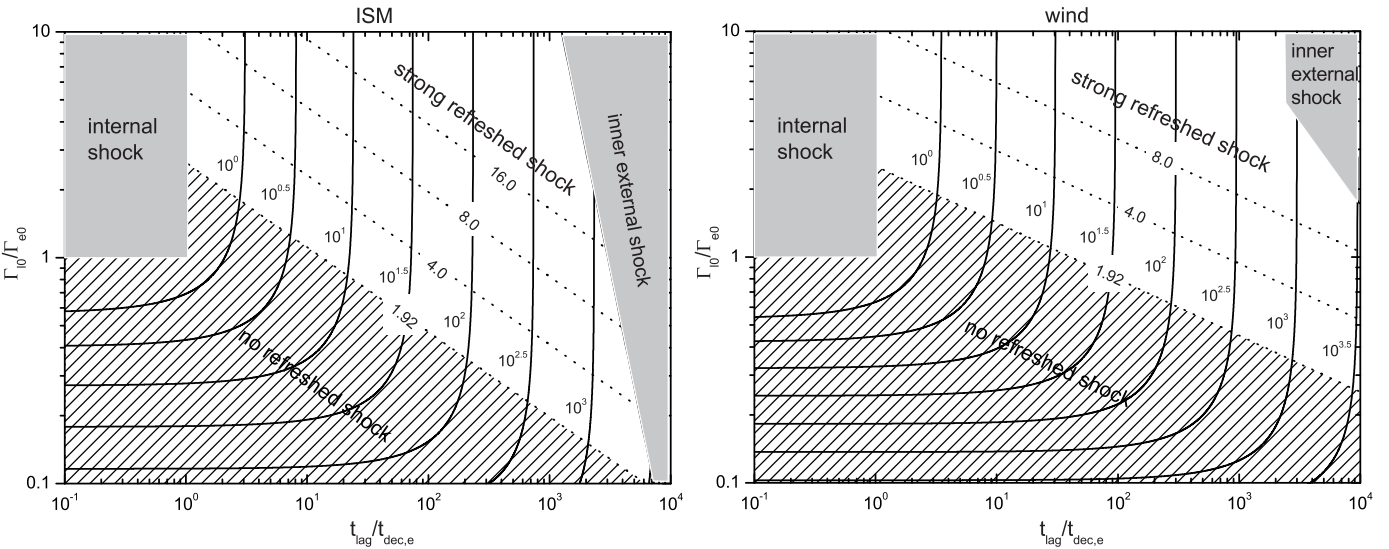


FIG. 3.— Three types of collision when the late ejecta catches up with the early ejecta, depending on the ratio of Γ_{l0} to Γ_{e0} and t_{lag} (which is scaled to the deceleration time of the early ejecta). Left and right panels correspond to two kinds of circum burst environment, i.e., the interstellar medium (left) and the free wind (right). The upper left grey region in each figure denotes the region for internal shocks. We simply neglect the width Δ_{e0} of the early ejecta. The right grey region (plotted assuming $\Gamma_{e0} = 100$, $E_l = 0.1E_e$) denotes the inner external shock region, in which the late ejecta can be decelerated in the non-relativistic tail of the early external shock. The rest region is for refreshed shocks. Different solid lines correspond to different values of $t_{\text{col}}/t_{\text{dec},e}$, ranging from 1 to $\sim 10^4$ as marked beside each line. Different dotted lines correspond to different values of $\Gamma_{l0}/\Gamma_e(R_{\text{col}})$, which are marked on the lines. If $\Gamma_{l0}/\Gamma_e(R_{\text{col}}) < 1.92$, the refreshed shock is suppressed by the thermal energy in the outer external shock.

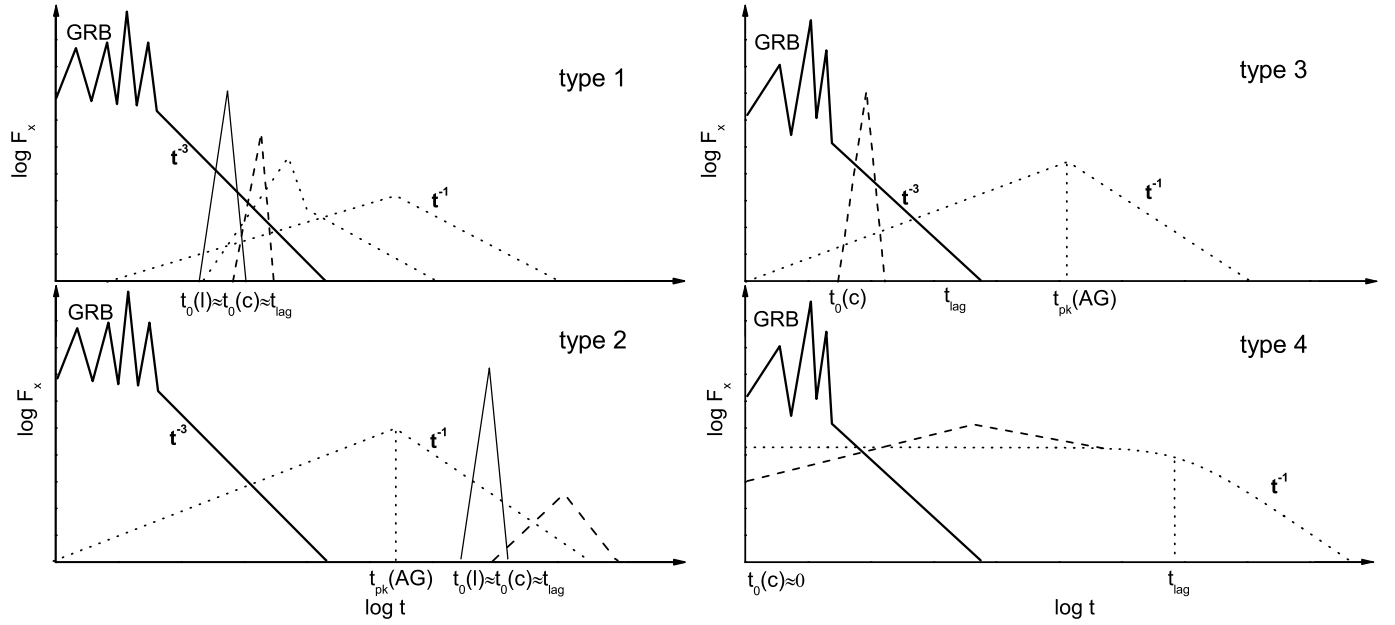


FIG. 4.— Four types of X-ray light curves, depending on the prompt GRB produced by internal shocks within the early ejecta (*Types 1 & 2*) or by internal shocks within the late ejecta (*Types 3 & 4*). In each case, the X-ray light curve is further determined by whether the collision between the two ejecta happens earlier than the deceleration of the early ejecta (*Types 1 & 3*) or not (*Types 2 & 4*). Thick solid lines represent the X-ray emission during the prompt GRB phase. The decaying index of the tail emission of the prompt GRB is $-2 + \beta \sim -3$. Thin solid lines correspond to the X-ray emission produced by the internal shock of the late ejecta. Dashed lines correspond to the emission from the collision between the two ejecta, which can be either the direct internal shock (*Types 1 & 3*) or the refreshed shock (*Types 2 & 4*). Dotted lines correspond to the emission from the external shock.